Projected *d*-wave superconducting state: A fermionic projected entangled pair state study

Qi Yang [1,2] Xing-Yu Zhang,[1,2] Hai-Jun Liao [1,3,*] Hong-Hao Tu [4,†] and Lei Wang[1,3,‡]

[1]*Institute of Physics, Chinese Academy of Sciences, Beijing 100190, China*
[2]*University of Chinese Academy of Sciences, Beijing 100049, China*
[3]*Songshan Lake Materials Laboratory, Dongguan, Guangdong 523808, China*
[4]*Institute of Theoretical Physics, Technische Universität Dresden, 01062 Dresden, Germany*

We investigate the physics of projected *d*-wave pairing states using their fermionic projected entangled pair state (fPEPS) representation. First, we approximate a *d*-wave Bardeen-Cooper-Schrieffer state using the Gaussian fPEPS. Next, we translate the resulting state into fPEPS tensors and implement the Gutzwiller projection which removes double occupancy by modifying the local tensor elements. The tensor network representation of the projected *d*-wave pairing state allows us to evaluate physical quantities in the thermodynamic limit without employing the Gutzwiller approximation. Despite having very few variational parameters, such physically motivated tensor network states are shown to exhibit competitive energies for the doped *t-J* model. We expect that such construction offers useful initial states and guidance for variational tensor network calculations.

I. INTRODUCTION

The projected Bardeen-Cooper-Schrieffer (BCS) states play a prominent role in the studies of strongly correlated electrons [1]. The state is obtained by eliminating the double occupancies in the BCS wave function

$$|\Psi\rangle = P_G |\text{BCS}\rangle, \tag{1}$$

where $P_G = \prod_{\mathbf{i}}(1 - n_{\mathbf{i}\uparrow} n_{\mathbf{i}\downarrow})$ is the Gutzwiller projection operator which implements the projection. The state consists of resonating valence bonds (RVBs), which are believed to be relevant to superconducting cuprates [2–4], frustrated magnets [5], and a broad range of other phenomena in strongly correlated physics. Subsequent theoretical and numerical investigations show that the projected BCS state in Eq. (1) is indeed the low-energy candidate state of the relevant *t-J* models and exhibits similar features as observed in superconducting cuprates [6–11].

To account for further intricacies such as competing orders, the vanilla RVB state [4] has developed into a full-fledged variational wave function [12–16]. Along with developments of other numerical methods [17–24], a point has been reached where uncertainties in the model Hamiltonian are even larger than the achieved accuracy of a many-body solver. The situation calls for more realistic models with inputs from *ab initio* calculations and experiments. In the meantime, it is worth pursuing deeper synergy between different methods beyond simply cross-checking their numerical data [18]. Such synergy will bridge the worlds of "educated guess of wave functions" and "solving Hamiltonians numerically," potentially offering more physical understandings.

An example of such promising synergy is to cast the family of projected BCS states into tensor network states. Recently, a number of works have developed methods for converting projected fermionic states into matrix product states [25–34] and used such translation to inspect state fidelity, study their entanglement properties, and facilitate density-matrix renormalization group calculations.

Extending this progress to convert projected fermionic states into two-dimensional tensor networks is highly desirable as this will allow one to investigate projected BCS states using methods from the tensor network toolbox. Along this line, there have been works constructing tensor network representations of the RVB states based on their real space picture [35–37]. In this work, we present a more generic approach which is based on the Gaussian fermionic projected entangled pair state (fPEPS) [38] and has a variable number of parameters to achieve the translation. Then we use it to investigate the projected *d*-wave pairing state in an infinite two-dimensional lattice.

Our starting point is a fermionic quadratic Hamiltonian with *d*-wave pairing on the two-dimensional (2D) square lattice,

$$H_{\text{BCS}} = \sum_{\mathbf{k},\sigma} \xi_{\mathbf{k}} f^{\dagger}_{\mathbf{k}\sigma} f_{\mathbf{k}\sigma} + \sum_{\mathbf{k}} (\Delta_{\mathbf{k}} f^{\dagger}_{\mathbf{k}\uparrow} f^{\dagger}_{-\mathbf{k}\downarrow} + \Delta^{*}_{\mathbf{k}} f_{-\mathbf{k}\downarrow} f_{\mathbf{k}\uparrow}), \tag{2}$$

where $f_{\mathbf{k}\sigma}$ ($f^{\dagger}_{\mathbf{k}\sigma}$) is the fermion annihilation (creation) operator in momentum space with spin index $\sigma = \uparrow, \downarrow$; $\xi_{\mathbf{k}} = -2t(\cos k_x + \cos k_y) - \mu$; and $\Delta_{\mathbf{k}} = 2\Delta_d(\cos k_x - \cos k_y)$. The hopping amplitude t is set to unity. The state $|\text{BCS}\rangle$ is the ground state of H_{BCS} parametrized by the chemical potential μ and the *d*-wave pairing amplitude Δ_d.

*navyphysics@iphy.ac.cn
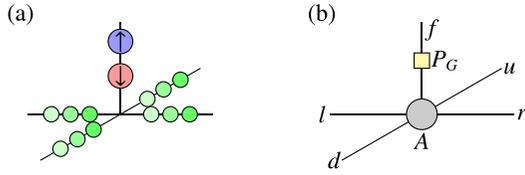†hong-hao.tu@tu-dresden.de
‡wanglei@iphy.ac.cn

FIG. 1. (a) The local fiducial state in Eq. (5) of a fPEPS. It is a state formed by the physical fermions of spin up and down (blue and red dots) and Λ flavors of virtual fermions reside on the bond (green dots). The state is fully characterized by the local correlation matrix in Eq. (6) if it is Gaussian. (b) Gutzwiller projection to the local fPEPS tensor.

Given the BCS Hamiltonian in Eq. (2), we first find a Gaussian fPEPS approximation to the pairing state $|\text{BCS}\rangle$ via a variational calculation. As shown in Fig. 1(a), the Gaussian fPEPS is formed by the physical fermions of spin up and down (blue and red dots) and Λ flavors of virtual fermions residing on each bond (green dots). Next, we translate the Gaussian fPEPS, parametrized by its correlation matrix, to fPEPS tensors and implement the Gutzwiller projection by locally modifying the tensor elements. Having an approximated fPEPS representation of the projected BCS state in Eq. (1) allows us to investigate its properties using tensor network algorithms. We examine the validity of the Gutzwiller approximation for the hole fugacity and report on the pairing order parameter and variational energy of the projected d-wave pairing state for the t-J model with various dopings.

II. METHOD

In this section, we present our method for obtaining the fPEPS tensors of a projected BCS state and the workflow is shown in Fig. 2. This section is organized as follows: We first review the construction of Gaussian fPEPS [38] in Sec. II A and the variational optimization of the Gaussian fPEPS [39] in Sec. II B. Then we develop the method to cast the
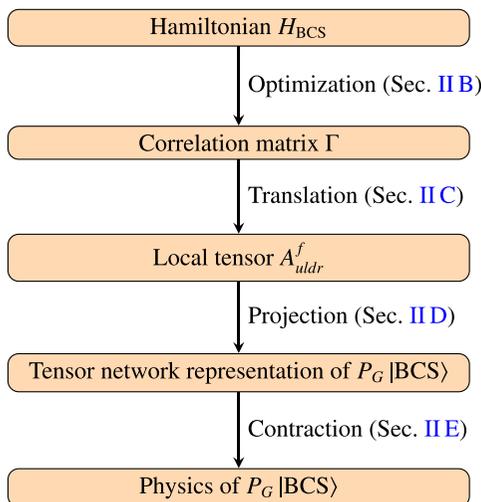

FIG. 2. The recipe for preparing a Gutzwiller projected BCS state in Eq. (1) as a fermionic PEPS and investigating its physical properties via tensor network contraction.

Gaussian fPEPS to fPEPS tensors and implement the Gutzwiller projection in Sec. II C and Sec. II D, respectively. Finally, in Sec. II E, we discuss how to make the fPEPS tensor obtained in Sec. II D compatible with the method of contracting fPEPS tensors developed in Ref. [40].

A. Construction of Gaussian fPEPS

The fPEPS is formed by mediating the entanglement of physical fermions (f) on lattice sites via virtual fermions (u, l, d, r) residing on the bonds. Formally, it can be expressed as [38,41]

$$|\Psi\rangle = \left[\bigotimes_{\langle \mathbf{i},\mathbf{j}\rangle} \langle \omega_{\mathbf{ij}}|\right]\left[\bigotimes_{\mathbf{i}} |A_{\mathbf{i}}\rangle\right], \qquad (3)$$

where $|\omega_{\mathbf{ij}}\rangle$ is a maximally entangled state of virtual fermions on the $\langle \mathbf{i}, \mathbf{j}\rangle$ bond. More concretely, we use $u_{\mathbf{i}\alpha}, l_{\mathbf{i}\alpha}, d_{\mathbf{i}\alpha}, r_{\mathbf{i}\alpha}$ to denote the annihilation operators of the virtual fermions at site $\mathbf{i}$, where $\alpha \in [1, \ldots, \Lambda]$ is the flavor index and u, l, d, r refer to up, left, down, and right, respectively. The horizontal bond between two neighboring sites $\mathbf{i}$ and $\mathbf{j} = \mathbf{i} + \hat{\mathbf{x}}$ is defined by

$$|\omega_{\mathbf{ij}}\rangle = \prod_{\alpha=1}^{\Lambda} \frac{1}{\sqrt{2}}(1 + r_{\mathbf{i}\alpha}^\dagger l_{\mathbf{j}\alpha}^\dagger)|\text{vac}\rangle, \qquad (4)$$

where $|\text{vac}\rangle$ is the vacuum of virtual fermions. The vertical bonds are defined in a similar way.

Next, the local fiducial state [41] is generally expressed as

$$|A_{\mathbf{i}}\rangle = \sum_{f,u,l,d,r} A_{uldr}^f |f\rangle \otimes |uldr\rangle, \qquad (5)$$

where $|f\rangle$ denotes the local physical states, consisting of empty, singly occupied (with either spin up or down), and doubly occupied states. The basis $|uldr\rangle$ corresponds to the Fock space of virtual fermions at site $\mathbf{i}$.

Since the virtual bonds are fermionic Gaussian states, the fPEPS in Eq. (3) would also be Gaussian, as long as the local fiducial state $|A_{\mathbf{i}}\rangle$ in Eq. (5) is a fermionic Gaussian state. Such a state forms a subclass of fPEPS, namely the Gaussian fPEPS [38]. The flavor number of virtual fermions controls the expressibility of the Gaussian fPEPS. In the usual fPEPS language, a Gaussian fPEPS with flavor number Λ has a bond dimension $D = 2^\Lambda$.

A great computational advantage of the Gaussian fPEPS is that a powerful fermionic Gaussian formalism [42] can be used for performing efficient computations, which we briefly outline below. Throughout this work we consider translationally invariant fPEPS on the 2D square lattice with a one-site unit cell (generalization to multisite unit cells and/or other lattices is straightforward though). Let us omit the site index for now and label the physical and virtual fermions at a local site as $(c_1, c_2, c_3, \ldots, c_{4\Lambda+2}) = (f_\uparrow, f_\downarrow, r_1, l_1, r_2, l_2, \ldots, r_\Lambda, l_\Lambda, d_1, u_1, d_2, u_2, \ldots, d_\Lambda, u_\Lambda)$. In terms of Majorana operators $\gamma_{2\mu-1} = c_\mu^\dagger + c_\mu$ and $\gamma_{2\mu} = -i(c_\mu^\dagger - c_\mu)$, the local fiducial state (5), being a fermionic Gaussian state, is fully characterized by its correlation matrix [42]

$$\Gamma_{\mu\nu} = \frac{i}{2}\langle A|[\gamma_\mu, \gamma_\nu]|A\rangle, \qquad (6)$$

where Γ is a real antisymmetric matrix satisfying $\Gamma^2 = -\mathbb{I}_{(8\Lambda+4)\times(8\Lambda+4)}$. As such, the correlation matrix (6) can be written as

$$\Gamma = \begin{pmatrix} A & B \\ -B^T & D \end{pmatrix}, \tag{7}$$

where A and D are 4×4 and $8\Lambda \times 8\Lambda$ real antisymmetric matrices, respectively, and B is a $4 \times 8\Lambda$ real matrix.

In a translationally invariant setup, both physical and virtual Majorana modes can be transformed into modes in momentum space with $\gamma_{\mathbf{k},\mu} = \frac{1}{\sqrt{N}} \sum_{\mathbf{j}} \exp(-i\mathbf{k} \cdot \mathbf{j})\gamma_{\mathbf{j},\mu}$ where $N = L^2$ is the total number of sites (L: number of sites along $\mathbf{x}$ and $\mathbf{y}$ directions). The allowed values of $\mathbf{k}$ satisfy $\mathbf{k} = \frac{2\pi\mathbf{n}}{L}$ where $\mathbf{n} \in \mathbb{Z} \oplus (\mathbb{Z} + \frac{1}{2})$ if the system has periodic (antiperiodic) boundary condition along the $\mathbf{x}$ ($\mathbf{y}$) direction [43]. Denoting the virtual bond state as $|\omega\rangle = \bigotimes_{\langle\mathbf{i},\mathbf{j}\rangle} |\omega_{\mathbf{ij}}\rangle$, the correlation matrix of the virtual bond state is written as $(G_{\mathbf{k}}^\omega)_{\mu\nu} = \frac{i}{2}\langle\omega|[\gamma_{\mathbf{k},\mu}, \gamma_{-\mathbf{k},\nu}]|\omega\rangle$ $(\mu, \nu = 5, \dots, 8\Lambda + 4)$ and takes the following explicit form [39]:

$$G_{\mathbf{k}}^\omega = \left[\bigoplus_{\mu=1}^{\Lambda} \begin{pmatrix} & e^{ik_x\sigma^x} \\ -e^{-ik_x\sigma^x} & \end{pmatrix}\right]$$
$$\oplus \left[\bigoplus_{\mu=1}^{\Lambda} \begin{pmatrix} & e^{ik_y\sigma^x} \\ -e^{-ik_y\sigma^x} & \end{pmatrix}\right], \tag{8}$$

where σ^x is the Pauli matrix.

The correlation matrix of the Gaussian fPEPS (3), defined by

$$\left(G_{\mathbf{k}}^{\mathrm{f}}\right)_{\mu\nu} = \frac{i}{2}\langle\Psi|[\gamma_{\mathbf{k},\mu}, \gamma_{-\mathbf{k},\nu}]|\Psi\rangle, \quad (\mu, \nu = 1, \dots, 4), \tag{9}$$

is calculated by contracting the virtual modes and gives rise to [38]

$$G_{\mathbf{k}}^{\mathrm{f}} = A + B(D + G_{\mathbf{k}}^\omega)^{-1}B^T. \tag{10}$$

This is a key result for the variational calculation below. We provide a comprehensive proof of Eq. (10) in Appendix A.

B. Variational optimization of Gaussian fPEPS

For the next step, we determine an optimal Gaussian fiducial state (5), such that the variational energy of the Hamiltonian H_{BCS} [see Eq. (2)] is minimized within the family of Gaussian fPEPS for a given flavor number Λ. The BCS ground state of H_{BCS} is thus approximated by a Gaussian fPEPS. By using the correlation matrix in Eq. (9), the variational energy can be expressed as

$$\langle H_{\mathrm{BCS}}\rangle = \sum_{\mathbf{k}} \xi_{\mathbf{k}}(\rho_{\mathbf{k}\uparrow} + \rho_{\mathbf{k}\downarrow}) + \Delta_{\mathbf{k}}\eta_{\mathbf{k}} + \Delta_{\mathbf{k}}^*\eta_{\mathbf{k}}^* \tag{11}$$

with $\rho_{\mathbf{k}\sigma} = \langle f_{\mathbf{k}\sigma}^\dagger f_{\mathbf{k}\sigma}\rangle$ and $\eta_{\mathbf{k}} = \langle f_{\mathbf{k}\uparrow}^\dagger f_{-\mathbf{k}\downarrow}^\dagger\rangle$, which can be evaluated via the relation $\sum_{\mathbf{k}} \xi_{\mathbf{k}}\langle f_{\mathbf{k}\uparrow}^\dagger f_{\mathbf{k}\uparrow}\rangle = \sum_{\mathbf{k}} \xi_{\mathbf{k}}[\frac{1}{2} - \frac{1}{2}(G_{\mathbf{k}}^{\mathrm{f}})_{1,2}]$, $\sum_{\mathbf{k}} \xi_{\mathbf{k}}\langle f_{\mathbf{k}\downarrow}^\dagger f_{\mathbf{k}\downarrow}\rangle = \sum_{\mathbf{k}} \xi_{\mathbf{k}}[\frac{1}{2} - \frac{1}{2}(G_{\mathbf{k}}^{\mathrm{f}})_{3,4}]$, and $\eta_{\mathbf{k}} = \langle f_{\mathbf{k}\uparrow}^\dagger f_{-\mathbf{k}\downarrow}^\dagger\rangle = \frac{1}{4}[(G_{\mathbf{k}}^{\mathrm{f}})_{1,4} + (G_{\mathbf{k}}^{\mathrm{f}})_{2,3} + i(G_{\mathbf{k}}^{\mathrm{f}})_{2,4} - i(G_{\mathbf{k}}^{\mathrm{f}})_{1,3}]$.

We carry out the optimization following Ref. [39]. The minimization is performed through the fiducial state's correlation matrix Γ in Eq. (7), which can be brought into a canonical form

$$\Gamma = X^T \left[\bigoplus_{\eta=1}^{4\Lambda+2} \begin{pmatrix} 0 & 1 \\ -1 & 0 \end{pmatrix}\right] X, \tag{12}$$

where X is an orthogonal matrix. The matrices A, B, D in Eq. (7) are hence functions of X, and so are the correlation matrix $G_{\mathbf{k}}^f$ in Eq. (10) and the variational energy in Eq. (11).

We optimize the real orthogonal matrix X by minimizing the loss function using optimization on the Stiefel manifold. The derivatives are calculated by using automatic differentiation with JAX [44]. The optimization algorithm is the conjugate gradient method offered by PYMANOPT [45]. This calculation was done for a finite lattice in the momentum space. Since the computational complexity scales linearly with the system size, one can reach pretty large systems easily [39]. The accuracy of such variational calculation can be verified by comparing the results with the exact solution of the BCS Hamiltonian.

C. Translation of correlation matrix Γ into local tensor

To obtain the local tensor of Gaussian fPEPS $A_{uldr}^f = \langle f| \otimes \langle uldr|A_{\mathbf{i}}\rangle$ [see Eq. (5)], we need to find out the fiducial state $|A_{\mathbf{i}}\rangle$ based on its correlation matrix Γ.

To this end, we simply construct a single-site fiducial Hamiltonian

$$h = -\sum_{\mu\nu} i\Gamma_{\mu\nu}\gamma_\mu\gamma_\nu \tag{13}$$

using the correlation matrix for the fiducial state. This Hamiltonian is quadratic and contains $8\Lambda + 4$ types of physical and virtual Majorana fermions at a single site.

It is easy to prove that $|A_{\mathbf{i}}\rangle$ is the unique ground state of the fiducial Hamiltonian h. By using the orthogonal matrix defined in Eq. (12), the Majorana operators can be rotated into a new basis as $\gamma' = X\gamma$. Notice that $(X\Gamma X^T)_{\mu\nu} = \frac{i}{2}\langle A_{\mathbf{i}}| [\gamma_\mu', \gamma_\nu'] |A_{\mathbf{i}}\rangle = [\bigoplus_{\eta=1}^{4\Lambda+2} \begin{pmatrix} 0 & 1 \\ -1 & 0 \end{pmatrix}]_{\mu\nu}$, which shows that the Gaussian fiducial state $|A_{\mathbf{i}}\rangle$ satisfies $i\gamma_{2m-1}'\gamma_{2m}' |A_{\mathbf{i}}\rangle = |A_{\mathbf{i}}\rangle$ $(m = 1, \dots, 4\Lambda + 2)$. As $i\gamma_{2m-1}'\gamma_{2m}'$ is a fermion parity operator and has eigenvalues ± 1, the fiducial Hamiltonian $h = -i\sum_m \gamma_{2m-1}'\gamma_{2m}' = -\sum_{\mu\nu} i\Gamma_{\mu\nu}\gamma_\mu\gamma_\nu$ has $|A_{\mathbf{i}}\rangle$ as its unique ground state.

We convert the fiducial Hamiltonian h from the Majorana basis to the original complex fermion basis [see Eq. (5)] and find its ground state by diagonalizing h. By reshaping the state vector $\in \mathbb{C}^{2^{4\Lambda+2}}$ into a five-leg tensor, we obtain A_{uldr}^f up to an unimportant overall phase.

Since the quadratic Hamiltonian conserves the fermion parity, its ground state $|A_{\mathbf{i}}\rangle$ has a definite parity. Therefore, the tensor A_{uldr}^f automatically inherits $\mathbb{Z}_2$ symmetry as the parity of the state $|A_{\mathbf{i}}\rangle$.

For obtaining the explicit form of $|A_{\mathbf{i}}\rangle$, an exact diagonalization of the fiducial Hamiltonian h is managable when the number of physical and virtual modes at each site is relatively small. This is indeed the case for our benchmark example, which already shows good performance. When the number of modes at each site is large, we provide a more efficient approach based on the state overlap in Appendix B.

D. Gutzwiller projection of Gaussian fPEPS

After obtaining a Gaussian fPEPS representation of the BCS state, we implement the Gutzwiller projection on the physical leg of the local tensor A^f_{uldr} as shown in Fig. 1(b). Since we carry out Gutzwiller projection in an infinite system in the grand canonical ensemble, we include a fugacity term in the empty configuration to account for the change of the particle density caused by the removal of double occupancies [46–49]. In this way, the projection operator reads

$$P_G = \prod_{\mathbf{i}} z^{(1-n_{\mathbf{i}\uparrow}-n_{\mathbf{i}\downarrow})/2}(1 - n_{\mathbf{i}\uparrow}n_{\mathbf{i}\downarrow}), \qquad (14)$$

where z is the fugacity of holes. The Gutzwiller projection operator is a local gate acting on the physical leg with the matrix representation $\mathrm{diag}(\sqrt{z}, 1, 1, 0)$, where the basis of this representation is $(|0\rangle, |\uparrow\rangle, |\downarrow\rangle, |\uparrow\downarrow\rangle)$. The zero in the Gutzwiller projection gate sets the local tensor elements associated with doubly occupied physical fermions to zero.

In principle, in a grand canonical calculation, one needs to tune the hole fugacity to maintain the average particle number. The Gutzwiller approximation [47] provides an estimation of the fugacity

$$z = \frac{2\delta}{1 + \delta}, \qquad (15)$$

where δ is the hole density. One sees that in the undoped case, $\delta = 0$, the projection removes both empty and double occupancy configurations and only keeps singly occupied sites.

E. Tensor network contraction

The Gaussian fPEPS after the Gutzwiller projection is no longer a Gaussian state, but preserves the fPEPS nature. To investigate its physical properties, we employ tensor network contraction algorithms for fPEPS [40]. Since the optimization in Sec. II B can be done on a sufficiently large lattice, it is essentially free of finite-size error. Thus, after translation and Gutzwiller projection, we assemble the local tensors into an infinite lattice and employ infinite tensor network contraction algorithms. Note that one needs to take care of the swap gate [50] when contracting the local tensors since it is a fermionic tensor network.

To make the local tensor fully compatible with the diagrammatic notation for fPEPS in Ref. [40], one should pay special attention to the fermion sign associated with the order and form of virtual fermions in the definition of $|A_{\mathbf{i}}\rangle$ and $|\omega_{\mathbf{ij}}\rangle$.

For example, we need to make sure that the order of fermionic operators in the definition of $|A_{\mathbf{i}}\rangle$ in Gaussian fPEPS and fPEPS are the same. In Ref. [40], the ordering of fermions in the local tensor is $|ulfdr\rangle$, while the tensor we obtained in Sec. II C follows the order $(c_1, c_2, \ldots, c_{4\Lambda+2}) = (f_\uparrow, f_\downarrow, r_1, l_1, r_2, l_2, \ldots, r_\Lambda, l_\Lambda, d_1, u_1, d_2, u_2, \ldots, d_\Lambda, u_\Lambda)$. In order to account for this difference, we introduce swap gates to transform between these two different orderings.

Additionally, in Ref. [40] it is free to contract the virtual bonds of two nearby fPEPS tensors without generating swap gates. This implies that the adopted definition of virtual fermion maximally entangled state is defined differently from Eq. (4). For example, for the bond between site $\mathbf{i}$ and

$\mathbf{j} = \mathbf{i} + \hat{\mathbf{x}}$, one has

$$|\omega^{\mathrm{C}}_{\mathbf{ij}}\rangle = \frac{1}{\sqrt{2^\Lambda}} \sum_{\{n_\alpha\}} \prod_{\alpha=1}^{\Lambda} (r^\dagger_{\mathbf{i}\alpha})^{n_\alpha} \prod_{\alpha=1}^{\Lambda} (l^\dagger_{\mathbf{j}\alpha})^{n_\alpha} |\mathrm{vac}\rangle, \qquad (16)$$

where $n_\alpha \in \{0, 1\}$ is the occupation number of virtual fermions.

This differs from Eq. (4) by the ordering of virtual fermions if the flavor number $\Lambda > 1$. The differences between $|\omega^{\mathrm{C}}_{\mathbf{ij}}\rangle$ and $|\omega_{\mathbf{ij}}\rangle$ can be expressed explicitly as

$$|\omega^{\mathrm{C}}_{\mathbf{ij}}\rangle = (-1)^{\sum_\alpha^\Lambda \sum_{\beta<\alpha}^\Lambda (r^\dagger_{\mathbf{i}\alpha} r_{\mathbf{i}\alpha})(l^\dagger_{\mathbf{j}\beta} l_{\mathbf{j}\beta})} |\omega_{\mathbf{ij}}\rangle \qquad (17)$$

for the neighboring sites $\mathbf{i}$ and $\mathbf{j} = \mathbf{i} + \hat{\mathbf{x}}$. For the case of $\mathbf{j} = \mathbf{i} + \hat{\mathbf{y}}$, $r_{\mathbf{i}\alpha}$ and $l_{\mathbf{j}\alpha}$ are replaced by $u_{\mathbf{i}\alpha}$ and $d_{\mathbf{j}\alpha}$, respectively.

All coefficients in Eq. (17) can be absorbed into the local tensor A^f_{uldr}. Afterward, the tensor network state is compatible with the fPEPS convention in Ref. [40] and the resulting local tensor is suitable for an fPEPS tensor contraction code.

To compute expectation values, we consider an infinite fPEPS and adopt the variational uniform matrix product state method [51] to obtain the environment tensors of infinite tensor networks [52]. We note that other methods (e.g., corner transfer matrix renormalization group method [53,54]) are also applicable.

III. RESULTS

The BCS Hamiltonian in Eq. (2) has Dirac points at $\mathbf{k} = (\pm\frac{\pi}{2}, \pm\frac{\pi}{2})$. When optimizing Γ, we choose a suitable combination of the system size L and boundary condition to avoid these exact zero modes, as we mentioned in Sec. II A.

First, as a sanity check, the expectation value of the Hamiltonian in Eq. (2) is calculated from optimized Gaussian fPEPS. The expectation value can be obtained in two different ways. The first way is through tensor network contraction, and the second way is using the correlation matrix [see Eq. (11)]. The result in Fig. 3 shows that the energies evaluated in these two ways agree with each other. The small discrepancy is due to the finite bond dimension of environments in the tensor network contraction. Such discrepancy can be reduced systematically by enlarging the bond dimension kept in the contraction.

Next, we move on to the Gutzwiller projected states. We denote the density of holes of unprojected fPEPS as δ and that of Gutzwiller projected state as δ_G, respectively. With a suitable choice of hole fugacity z, we expect $\delta = \delta_G$. Here, we examine the Gutzwiller approximated fugacity $z = 2\delta/(1 + \delta)$ [47]. The result in Fig. 4 shows that the approximated fugacity is smaller than needed since δ is larger than δ_G. Thus, the fugacity should be enlarged to make sure that δ remains unchanged after the Gutzwiller projection.

The projected d-wave pairing state is believed to be a good candidate for the ground state of the t-J model [4] with the Hamiltonian [56,57]

$$H_{tJ} = -t \sum_{\langle \mathbf{i},\mathbf{j}\rangle, \sigma} P_G(f^\dagger_{\mathbf{i}\sigma} f_{\mathbf{j}\sigma} + \mathrm{H.c.})P_G + J \sum_{\langle \mathbf{i},\mathbf{j}\rangle} \left(\mathbf{S}_{\mathbf{i}} \cdot \mathbf{S}_{\mathbf{j}} - \frac{n_{\mathbf{i}}n_{\mathbf{j}}}{4}\right), \qquad (18)$$

where $\mathbf{S}_{\mathbf{i}} = \frac{1}{2}\sum_{ab} f^\dagger_{\mathbf{i},a} \boldsymbol{\sigma}_{ab} f_{\mathbf{i},b}$ and $n_{\mathbf{i}} = \sum_\sigma f^\dagger_{\mathbf{i}\sigma} f_{\mathbf{i}\sigma}$ are spin and charge density operators, respectively. We set $J/t = 0.4$ ($t =$
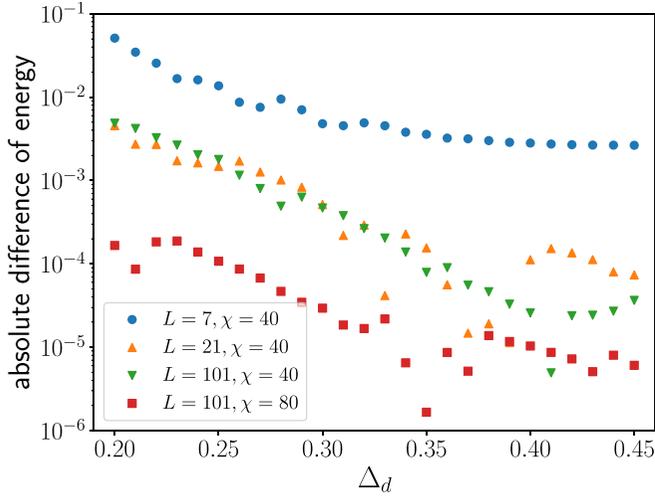
FIG. 3. Absolute difference of energy between those obtained from the correlation matrix of Gaussian fPEPS and direct tensor network contraction of an infinite fPEPS. The hole density is set to $\delta = 0.16$ and the virtual fermion flavor number in the Gaussian fPEPS is $\Lambda = 2$. χ is the bond dimension used in the variational uniform matrix product state algorithm [51]. This result reveals that for small system size, the difference mainly comes from the finite-size effect of Gaussian fPEPS and can be minimized by enlarging system size. If the system size is large enough, the difference comes from the finite bond dimension of environments in contraction. Nevertheless, the difference is quite small.

1) and carry out a variational calculation with the Gutzwiller projected *d*-wave ansatz.

Treating Δ_d in Eq. (2) as the single variational parameter, we need to optimize the variational energy of H_{tJ} (denoted as E_{tJ}) for each given hole concentration δ_G. In the calculation, it is crucial to keep the same δ_G when varying Δ_d since the variational energy is very sensitive to δ_G. We achieve this by
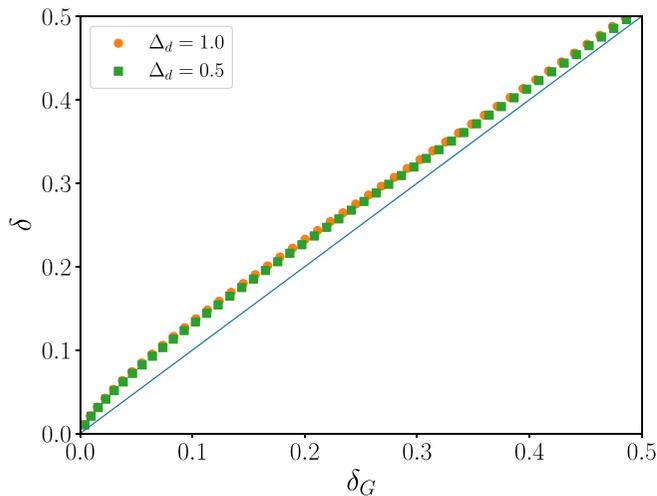

FIG. 5. The density of charge and pairing strength of the Gutzwiller projected BCS state in the case of $\Lambda = 2$, $\delta = 0.16$, $\Delta_d = 0.25$. The diameter of red circles scales with the quantity of density of holes. The width of cyan and green lines scales with the absolute value of pairing strength where the sign of the pairing strength is positive (negative) for the cyan (green) lines.

tuning the fugacity using a bisection search as an inner loop for the variational optimization of Δ_d.

Figure 5 shows the measured correlations for an optimized state. The state is uniform and does not exhibit magnetic or charge order but hosts a *d*-wave superconducting order.

Directly observing a perfect dome shape in the order parameter $\frac{1}{\sqrt{2}}|\langle f_{\mathbf{i}\uparrow} f_{\mathbf{j}\downarrow} - f_{\mathbf{i}\downarrow} f_{\mathbf{j}\uparrow}\rangle|$ for neighboring sites $\mathbf{i}, \mathbf{j}$ is difficult for some reasons. The convergence of the variational uniform matrix product state algorithm is difficult for small Δ_d and δ_G. Thus, the range of investigated δ_G is limited to $(0.11, 0.16)$. Besides, the tensor network contraction error makes it difficult to find the optimal Δ_d and corresponding order parameter with high precision. As an outlook, it might be possible to improve the convergence and precision by exploiting the SU(2) symmetry of the fPEPS in tensor network contractions [58].

As the bisection search of z is unaffordable for $\Lambda = 3$, we investigate the order parameter for $\Lambda = 2$. As shown in Fig. 6, in the limited range of δ_G, the optimal variational parameter Δ_d decreases with doping and the pairing order parameter increases with doping. On the other hand, the order parameter increases with Δ_d for a fixed doping. Putting these three facts together, it can be expected that for larger δ_G, the

FIG. 4. Hole density before (δ) and after (δ_G) the Gutzwiller projection. Here, we consider $\Lambda = 2$ and $L = 101$. The deviation of points from the blue line represents the error of the Gutzwiller approximation for the hole fugacity in Eq. (15).
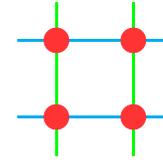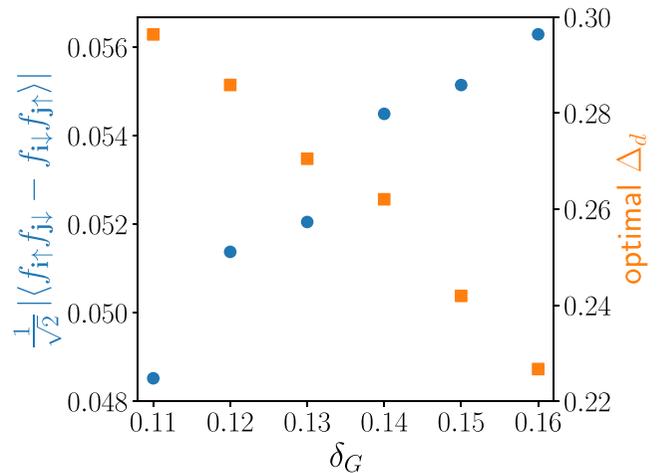

FIG. 6. Order parameter $\frac{1}{\sqrt{2}}|\langle f_{\mathbf{i}\uparrow} f_{\mathbf{j}\downarrow} - f_{\mathbf{i}\downarrow} f_{\mathbf{j}\uparrow}\rangle|$ (blue circle) for neighboring sites $\mathbf{i}, \mathbf{j}$ and optimal Δ_d (orange square) versus δ_G for $\Lambda = 2$ and $L = 101$. The order parameter is obtained by using the tensor network contraction. For stability, the optimal Δ_d is determined via a second degree polynomial fitting near the optimal points.
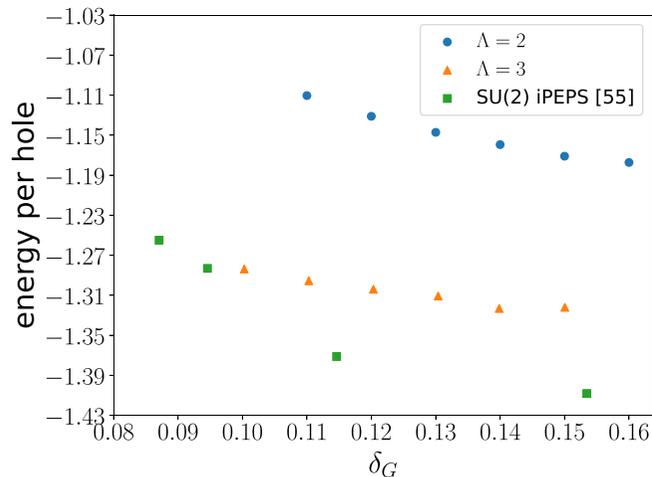
FIG. 7. Energy per hole. In $\Lambda = 2$ cases, we vary Δ_d to minimize the energy of the t-J model for a given density of holes δ_G. Fugacity in the Gutzwiller projector is tuned for each Δ_d to ensure the final δ_G be the same, which is crucial in finding optimized Δ_d. For $\Lambda = 3$ cases, we used optimized Δ_d and solved fugacity in $\Lambda = 2$ for each δ to avoid a costly optimization of Δ_d and solution of fugacity in $\Lambda = 3$. Green squares are from SU(2) fPEPS calculations in [55].

order parameter will decrease as the optimal Δ_d decreases with doping and finally drop to zero. In conclusion, one would obtain a dome shape in the order parameter versus doping.

Lastly, we compute the energy per hole ($E_{tJ} + 0.46778)/\delta_G$ for $\Lambda = 2$ and 3 where -0.46778 is the ground-state energy for the undoped case [59]. Increasing bond dimension results in a lower energy expectation value, reaching an energy per hole as low as -1.32. The energies are higher than those obtained from direct optimization of fPEPS in Refs. [17,55]. Figure 7 shows the energy per hole as a function of doping. We compare the energy with the SU(2) fPEPS results of Ref. [55] obtained at $D^* = 6$, which amounts to $D \approx 11$ without symmetry. Note that for $\Lambda = 3$, our fPEPS obtained from the Gutzwiller ansatz has bond dimension $D = 8$. Besides, our fPEPS tensor is uniform, while Ref. [55] uses a 2×2 or 5×2 unit cell. Constructing a tensor network representation of projected d-wave pairing states opens the way to provide good initial states in variational calculations besides offering diagnosis from the tensor network toolbox.

IV. SUMMARY AND DISCUSSION

To summarize, we have developed a systematic method to construct the fPEPS representation of projected BCS states. Using the method, we investigated the physical properties of the projected d-wave pairing state on an infinite square lattice. In particular, the estimated variational energy for the t-J model is comparable to the results from tensor network optimizations. The code implementation is available online [60].

Our approach can also be applied to other classes of projected fermionic states, such as those obtained from Chern insulators and spin density wave states [61]. In certain cases, one would need an enlarged unit cell in the construction and contraction of tensor networks. In contrast to previous works

[35–37,62–64] which rely on an analytical PEPS representation of the RVB state, the present approach variationally solves a fermionic quadratic Hamiltonian of unprojected states using Gaussian fPEPS [39]. Thus, the present approach has a broader range of applications and can be systematically improved by increasing the bond dimension of the Gaussian fPEPS tensor.

Partial Gutzwiller projection which suppresses but does not eliminate double occupancies [65] can also be straightforwardly implemented. These states are relevant to the study of Gossamer superconductors [66,67] and Hubbard models. In principle, long-range Jastrow factors beyond the on-site Gutzwiller projection can be applied by using its tensor network form [68]. This class of states is considered to be crucial for describing Mott transitions [69]. Further investigations of these states with our method are left for future works.

APPENDIX A: PROOF OF EQUATION (10)

To establish the relationship between the correlation matrix of the Gaussian fPEPS and that of the fiducial state in Eq. (6), we prove a general result below.

Let us consider a fermionic Gaussian state $|\omega\rangle$ living in the Hilbert space $\mathcal{H}_2$ with virtual Majorana modes d_l ($l = 1, \ldots, 2m$) and another fermionic Gaussian state $|A\rangle$ living in the composite Hilbert space $\mathcal{H}_1 \otimes \mathcal{H}_2$ including both physical and virtual Majorana modes [70], where the physical modes are denoted as c_j ($j = 1, \ldots, 2n$).

The overlap $\langle\omega|A\rangle$ is also a fermionic Gaussian state and lives in the physical Hilbert space $\mathcal{H}_1$. To calculate its correlation matrix, it is convenient to work with density operators and write the density operator of $\langle\omega|A\rangle$ as

$$\rho_f(c) = \langle\omega|A\rangle\langle A|\omega\rangle = \text{tr}_{\mathcal{H}_2}[\rho_A(c, d)\rho_\omega(d)], \quad \text{(A1)}$$

where $\text{tr}_{\mathcal{H}_2}$ is the partial trace over $\mathcal{H}_2$ and ρ_ω (ρ_A) is the density operator of $|\omega\rangle$ ($|A\rangle$).

We shall establish a Grassmann integration approach to calculate the partial trace in Eq. (A1). This approach uses the Grassmann representations of the Gaussian density operators ρ_ω and ρ_A [42],

$$g_\omega(\tau) = \frac{1}{2^m} \exp\left(\frac{i}{2}\tau^T \Gamma_\omega \tau\right), \quad \text{(A2)}$$

and

$$g_A(\theta, \zeta) = \frac{1}{2^{n+m}} \exp\left[\frac{i}{2}(\theta^T \quad \zeta^T)\begin{pmatrix} A & B \\ -B^T & D \end{pmatrix}\begin{pmatrix} \theta \\ \zeta \end{pmatrix}\right], \quad \text{(A3)}$$

where $\theta = (\theta_1, \ldots, \theta_{2n})^T$ is a vector of real Grassmann variables for the physical modes $c = (c_1, \ldots, c_{2n})^T$ and, similarly, τ and ζ include Grassmann variables for virtual modes. Here Γ_ω and $\begin{pmatrix} A & B \\ -B^T & D \end{pmatrix}$ are the correlation matrices of ρ_ω and ρ_A, respectively.

In the Grassmann representation, the partial trace over $\mathcal{H}_2$ in Eq. (A1) can be calculated using a Grassmann integration as follows:

$$g_f(\theta) = (-2)^m \int D\zeta D\tau \, e^{\zeta^T \tau} g_A(\theta, \zeta) g_\omega(\tau), \quad \text{(A4)}$$

where $g_f(\theta)$ is the Grassmann representation of the (unnormalized) density operator for $\langle \omega | A \rangle$ and the integration is over Grassmann variables associated with virtual modes, with the notation $\int D\zeta D\tau = \int d\zeta_{2m} \cdots d\zeta_1 d\tau_{2m} \cdots d\tau_1$. The proof of (A4) is done by comparing the outcomes of Eqs. (A1) and (A4), where the former can be computed by expanding ρ_A and ρ_ω in terms of Majorana operators and performing the partial trace, and the latter is computed by expanding the Grassmann exponential and carrying out the integration over Grassmann variables one by one.

After substituting Eqs. (A2) and (A3) into Eq. (A4) and performing the Gaussian integration over ζ and τ, we obtain

$$g_f(\theta) = \frac{1}{2^{n+m}} \text{Pf}\,(\Gamma_\omega) \text{Pf}\,(D - \Gamma_\omega^{-1}) \exp\left(\frac{i}{2}\theta^T \Gamma_f \theta\right), \quad \text{(A5)}$$

where Pf denotes the Pfaffian for antisymmetric matrices and Γ_f is the correlation matrix of $\langle \omega | A \rangle$ and has the following explicit form:

$$\begin{aligned} \Gamma_f &= A + B(D - \Gamma_\omega^{-1})^{-1} B^T \\ &= A + B(D + \Gamma_\omega)^{-1} B^T. \end{aligned} \quad \text{(A6)}$$

Here we used $\Gamma_\omega^{-1} = -\Gamma_\omega$ as $|\omega\rangle$ is a pure state.

We note that Eq. (10) is just the Fourier transformed version of (A6) taking into account the translation invariance. It is also worth mentioning that Eq. (A6) agrees with Eq. (C8) in Ref. [71] but differs from those in Refs. [38,41,72] by the sign in front of Γ_ω. This is due to that the Gaussian fPEPS projector in Refs. [38,41,72] is defined through the Gaussian map [42], which is different from Eq. (3).

APPENDIX B: OVERLAP-BASED TRANSLATION

Instead of diagonalizing the fiducial Hamiltonian in the Fock space, we provide below an alternative approach to obtain the explicit tensor form of $|A_\mathbf{i}\rangle$. This approach is based on an overlap formula between fermionic Gaussian states and Fock states.

To start with, we rewrite the fiducial Hamiltonian (13) in a Bogoliubov–de Gennes (BdG) form by converting the Majorana operators γ back to original complex fermions,

$$H = (c^\dagger \quad c)\mathcal{H}\begin{pmatrix} c \\ c^\dagger \end{pmatrix}, \quad \text{(B1)}$$

where $(c^\dagger \quad c)$ is a row vector of fermionic creation and annihilation operators for $4\Lambda + 2$ physical and virtual fermions at a local site (see Sec. II A). The BdG single-particle Hamiltonian

$\mathcal{H}$ is diagonalized by a Bogoliubov transformation

$$(a^\dagger \quad a) = (c^\dagger \quad c)\begin{pmatrix} U & V^* \\ V & U^* \end{pmatrix}, \quad \text{(B2)}$$

where $(a^\dagger \quad a)$ includes creation and annihilation operators of Bogoliubov modes and the Bogoliubov matrices U and V satisfy

$$U^\dagger U + V^\dagger V = \mathbb{I}, \quad U^T V + V^T U = \mathbb{O} \quad \text{(B3)}$$

with $\mathbb{I}$ ($\mathbb{O}$) being the identity (zero) matrix.

The local fiducial state $|A_\mathbf{i}\rangle$, being the ground state of H, is annihilated by all a-fermion annihilation operators. According to Eq. (5), the tensor form of $|A_\mathbf{i}\rangle$ can be obtained by calculating each coefficient A_{uldr}^f which is the overlap $\langle f | \otimes \langle uldr | A_\mathbf{i} \rangle$. $\langle f | \otimes \langle uldr |$ denotes a Fock state in the c-fermion basis and can generally be written as $_c\langle 0 | c_{i_{M'}} \cdots c_{i_1}$ with $0 \leqslant M' \leqslant 4\Lambda + 2$ and $1 \leqslant i_1 < \cdots < i_{M'} \leqslant 4\Lambda + 2$, where $_c\langle 0 |$ is the c-fermion vacuum.

Such overlap calculation can be carried out by rewriting the Bogoliubov vacuum $|A_\mathbf{i}\rangle$ in a suitable form [73], with the help of the Bloch-Messiah decomposition [74]

$$\begin{pmatrix} U & V^* \\ V & U^* \end{pmatrix} = \begin{pmatrix} D & 0 \\ 0 & D^* \end{pmatrix}\begin{pmatrix} \bar{U} & \bar{V} \\ \bar{V} & \bar{U} \end{pmatrix}\begin{pmatrix} C & 0 \\ 0 & C^* \end{pmatrix}, \quad \text{(B4)}$$

where D and C are unitary matrices and $\bar{U}$ and $\bar{V}$ are real matrices with the following form:

$$\bar{U} = \begin{pmatrix} \mathbb{O} & \\ & \bigoplus_p u_p \sigma^0 \\ & & \mathbb{I} \end{pmatrix}, \quad \bar{V} = \begin{pmatrix} \mathbb{I} & \\ & \bigoplus_p i v_p \sigma^y \\ & & \mathbb{O} \end{pmatrix}. \quad \text{(B5)}$$

Here u_p and v_p are positive and satisfy $u_p^2 + v_p^2 = 1$, $\mathbb{I}$ ($\mathbb{O}$) is the identity (zero) matrix, and σ^0 and σ^y are the 2×2 identity and Pauli matrices. For our purpose, it is convenient to truncate the $\mathbb{I}$ ($\mathbb{O}$) block in $\bar{U}$ ($\bar{V}$) to obtain matrices

$$\bar{U}' = \begin{pmatrix} \mathbb{O} & \\ & \bigoplus_p u_p \sigma^0 \end{pmatrix}_{M \times M}, \quad \bar{V}' = \begin{pmatrix} \mathbb{I} & \\ & \bigoplus_p i v_p \sigma^y \end{pmatrix}_{M \times M}. \quad \text{(B6)}$$

Following Ref. [34], $|A_\mathbf{i}\rangle$ is represented as

$$|A_\mathbf{i}\rangle = \frac{1}{\prod_p v_p} b_1 \cdots b_M |0\rangle_c, \quad \text{(B7)}$$

where $b = c^\dagger D' \bar{V}' + c(D')^* \bar{U}'$. Here D' is a $(4\Lambda + 2) \times M$ matrix obtained by keeping the first M columns of the unitary matrix D [see Eq. (B4)], which is an isometry satisfying $(D')^\dagger D' = \mathbb{I}_{M \times M}$.

With these results in hand, the tensor entry A_{uldr}^f is calculated with Wick's theorem as follows:

$$\begin{aligned} \langle f | \otimes \langle uldr | A_\mathbf{i} \rangle &= \frac{1}{\prod_p v_p}\,_c\langle 0 | c_{i_{M'}} \cdots c_{i_1} b_1 \cdots b_M |0\rangle_c \\ &= \frac{(-1)^{\frac{1}{2}M'(M'-1)}}{\prod_p v_p}\,_c\langle 0 | c_{i_1} \cdots c_{i_{M'}} b_1 \cdots b_M |0\rangle_c \\ &= \frac{(-1)^{\frac{1}{2}M'(M'-1)}}{\prod_p v_p} \text{Pf}\begin{pmatrix} \mathbb{O}_{M' \times M'} & \mathbb{R}_{M' \times M} \\ -\mathbb{R}_{M \times M'}^T & \mathbb{Q}_{M \times M} \end{pmatrix}, \end{aligned} \quad \text{(B8)}$$

where $\mathbb{R}_{m'm} = {}_c\langle 0|c_{i_{m'}}b_m|0\rangle_c = (D'\bar{V}')_{i_{m'}m}$ and $\mathbb{Q}_{m'm} = {}_c\langle 0|b_{m'}b_m|0\rangle_c = (\bar{U}'\bar{V}')_{m'm}$. Note, however, that the overlap in Eq. (B8) vanishes if M and M' have different parity (this automatically encodes the fermion parity symmetry). The Pfaffian formula (B8) allows us to calculate the explicit tensor form of $|A_\mathbf{i}\rangle$. In our program, the Pfaffian is calculated with an algorithm provided by Wimmer [75].

We can compare the pros and cons of Hamiltonian-based translation and overlap-based translation: The complexity of translation is quantified by $N = 4\Lambda + 2$. When employing an overlap-based algorithm, we need to calculate matrix Pfaffians for 2^{N-1} times. As the size of each matrix is of order $2N \times 2N$, the computational cost of the overlap-based

translation is $O(N^3 \times 2^{N-1})$. This complexity can be further reduced to $O(N^2 \times 2^{N-1})$ if a fast update technique for the Pfaffian is used (see, e.g., Ref. [76]). Meanwhile, in the Hamiltonian-based algorithm, the computational cost of obtaining the dominant eigenvector of a $2^N \times 2^N$ matrix scales as $O((2^N)^2) = O(2^{2N})$.

When Λ is large, the Hamiltonian-based algorithm in Sec. II C has a larger computational cost, but it is nevertheless more straightforward and intuitive. If Λ is so large that an exact diagonalization of the fiducial Hamiltonian is not feasible, one might also employ the density matrix renormalization group method [77] to obtain an approximation of $|A_\mathbf{i}\rangle$.

[1] P. A. Lee, Rep. Prog. Phys. **71**, 012501 (2008).

[2] P. W. Anderson, Science **235**, 1196 (1987).

[3] G. Baskaran and P. W. Anderson, Phys. Rev. B **37**, 580 (1988).

[4] P. W. Anderson, P. A. Lee, M. Randeria, T. M. Rice, N. Trivedi, and F. C. Zhang, J. Phys.: Condens. Matter **16**, R755 (2004).

[5] P. Fazekas and P. W. Anderson, Philos. Mag. **30**, 423 (1974).

[6] F. C. Zhang, C. Gros, T. M. Rice, and H. Shiba, Supercond. Sci. Technol. **1**, 36 (1988).

[7] C. Gros, Phys. Rev. B **38**, 931 (1988).

[8] C. Gros, Ann. Phys. **189**, 53 (1989).

[9] H. Yokoyama and H. Shiba, J. Phys. Soc. Jpn. **57**, 2482 (1988).

[10] A. Paramekanti, M. Randeria, and N. Trivedi, Phys. Rev. Lett. **87**, 217002 (2001).

[11] B. Edegger, V. N. Muthukumar, and C. Gros, Adv. Phys. **56**, 927 (2007).

[12] H. Yokoyama and M. Ogata, J. Phys. Soc. Jpn. **65**, 3615 (1996).

[13] D. A. Ivanov, Phys. Rev. B **70**, 104503 (2004).

[14] M. Lugas, L. Spanu, F. Becca, and S. Sorella, Phys. Rev. B **74**, 165122 (2006).

[15] A. S. Darmawan, Y. Nomura, Y. Yamaji, and M. Imada, Phys. Rev. B **98**, 205132 (2018).

[16] T. Misawa, S. Morita, K. Yoshimi, M. Kawamura, Y. Motoyama, K. Ido, T. Ohgoe, M. Imada, and T. Kato, Comput. Phys. Commun. **235**, 447 (2019).

[17] P. Corboz, T. M. Rice, and M. Troyer, Phys. Rev. Lett. **113**, 046402 (2014).

[18] B. X. Zheng, C. M. Chung, P. Corboz, G. Ehlers, M. P. Qin, R. M. Noack, H. Shi, S. R. White, S. Zhang, and G. K. L. Chan, Science **358**, 1155 (2017).

[19] B. Ponsioen, S. S. Chung, and P. Corboz, Phys. Rev. B **100**, 195141 (2019).

[20] H.-C. Jiang and S. A. Kivelson, Phys. Rev. Lett. **127**, 097002 (2021).

[21] S. Gong, W. Zhu, and D. N. Sheng, Phys. Rev. Lett. **127**, 097003 (2021).

[22] S. Jiang, D. J. Scalapino, and S. R. White, Proc. Natl. Acad. Sci. USA **118**, e2109978118 (2021).

[23] M. Qin, C.-M. Chung, H. Shi, E. Vitali, C. Hubig, U. Schollwöck, S. R. White, and S. Zhang (Simons Collaboration on the Many-Electron Problem), Phys. Rev. X **10**, 031016 (2020).

[24] S. Sorella, arXiv:2101.07045.

[25] P. Silvi, D. Rossini, R. Fazio, G. E. Santoro, and V. Giovannetti, Int. J. Mod. Phys. B **27**, 1345029 (2013).

[26] M. P. Zaletel, Exact tensor network ansatz for strongly interacting systems, Ph.D. thesis, University of California, Berkeley, 2014.

[27] M. T. Fishman and S. R. White, Phys. Rev. B **92**, 075132 (2015).

[28] B. Bauer, B. P. Keller, S. Trebst, and A. W. W. Ludwig, Phys. Rev. B **99**, 035155 (2019).

[29] Y.-H. Wu, L. Wang, and H.-H. Tu, Phys. Rev. Lett. **124**, 246401 (2020).

[30] H.-K. Jin, H.-H. Tu, and Y. Zhou, Phys. Rev. B **101**, 165135 (2020).

[31] G. Petrica, B.-X. Zheng, G. K.-L. Chan, and B. K. Clark, Phys. Rev. B **103**, 125161 (2021).

[32] H.-K. Jin, H.-H. Tu, and Y. Zhou, Phys. Rev. B **104**, L020409 (2021).

[33] A. M. Aghaei, B. Bauer, K. Shtengel, and R. V. Mishmash, arXiv:2009.12435.

[34] H.-K. Jin, R.-Y. Sun, Y. Zhou, and H.-H. Tu, Phys. Rev. B **105**, L081101 (2022).

[35] F. Verstraete, M. M. Wolf, D. Perez-Garcia, and J. I. Cirac, Phys. Rev. Lett. **96**, 220601 (2006).

[36] D. Poilblanc, N. Schuch, D. Pérez-García, and J. I. Cirac, Phys. Rev. B **86**, 014404 (2012).

[37] D. Poilblanc, P. Corboz, N. Schuch, and J. I. Cirac, Phys. Rev. B **89**, 241106(R) (2014).

[38] C. V. Kraus, N. Schuch, F. Verstraete, and J. I. Cirac, Phys. Rev. A **81**, 052338 (2010).

[39] Q. Mortier, N. Schuch, F. Verstraete, and J. Haegeman, Phys. Rev. Lett. **129**, 206401 (2022).

[40] P. Corboz, R. Orús, B. Bauer, and G. Vidal, Phys. Rev. B **81**, 165104 (2010).

[41] T. B. Wahl, S. T. Haßler, H.-H. Tu, J. I. Cirac, and N. Schuch, Phys. Rev. B **90**, 115133 (2014).

[42] S. Bravyi, Quantum Inf. Comput. **5**, 216 (2005).

[43] Together with suitably chosen system sizes, this boundary condition avoids the complication of dealing with exact zero modes at the Dirac points $\mathbf{k} = (\pm\frac{\pi}{2}, \pm\frac{\pi}{2})$ of the d-wave pairing Hamiltonian.

[44] J. Bradbury, R. Frostig, P. Hawkins, M. J. Johnson, C. Leary, D. Maclaurin, G. Necula, A. Paszke, J. VanderPlas, S. Wanderman-Milne, and Q. Zhang, JAX: Composable

transformations of Python+NumPy programs, http://github.com/google/jax.

[45] J. Townsend, N. Koep, and S. Weichwald, J. Mach. Learn. Res. **17**, 1 (2016).

[46] B. A. Bernevig, R. B. Laughlin, and D. I. Santiago, Phys. Rev. Lett. **91**, 147003 (2003).

[47] B. Edegger, N. Fukushima, C. Gros, and V. N. Muthukumar, Phys. Rev. B **72**, 134504 (2005).

[48] P. Anderson and N. Ong, J. Phys. Chem. Solids **67**, 1 (2006).

[49] C.-P. Chou, F. Yang, and T.-K. Lee, Phys. Rev. B **85**, 054510 (2012).

[50] P. Corboz and G. Vidal, Phys. Rev. B **80**, 165129 (2009).

[51] V. Zauner-Stauber, L. Vanderstraeten, M. T. Fishman, F. Verstraete, and J. Haegeman, Phys. Rev. B **97**, 045145 (2018).

[52] B. Vanhecke, M. V. Damme, J. Haegeman, L. Vanderstraeten, and F. Verstraete, SciPost Phys. Core **4**, 004 (2021).

[53] T. Nishino and K. Okunishi, J. Phys. Soc. Jpn. **66**, 3040 (1997).

[54] R. Orús and G. Vidal, Phys. Rev. B **80**, 094403 (2009).

[55] J.-W. Li, B. Bruognolo, A. Weichselbaum, and J. von Delft, Phys. Rev. B **103**, 075127 (2021).

[56] F. C. Zhang and T. M. Rice, Phys. Rev. B **37**, 3759 (1988).

[57] M. Ogata and H. Fukuyama, Rep. Prog. Phys. **71**, 036501 (2008).

[58] J.-W. Li, J. von Delft, and H.-H. Tu, Phys. Rev. B **107**, 085148 (2023).

[59] A. W. Sandvik, Phys. Rev. B **56**, 11678 (1997).

[60] See https://github.com/TensorBFS/Gaussian-fPEPS.

[61] I. Affleck and J. B. Marston, Phys. Rev. B **37**, 3774 (1988).

[62] N. Schuch, D. Poilblanc, J. I. Cirac, and D. Pérez-García, Phys. Rev. B **86**, 115108 (2012).

[63] L. Wang, D. Poilblanc, Z.-C. Gu, X.-G. Wen, and F. Verstraete, Phys. Rev. Lett. **111**, 037202 (2013).

[64] S. Yang, T. B. Wahl, H.-H. Tu, N. Schuch, and J. I. Cirac, Phys. Rev. Lett. **114**, 106803 (2015).

[65] M. C. Gutzwiller, Phys. Rev. Lett. **10**, 159 (1963).

[66] R. B. Laughlin, Philos. Mag. **86**, 1165 (2006).

[67] F. C. Zhang, Phys. Rev. Lett. **90**, 207002 (2003).

[68] Z. Li, M. J. O'Rourke, and G. K.-L. Chan, Phys. Rev. B **100**, 155121 (2019).

[69] M. Capello, F. Becca, M. Fabrizio, S. Sorella, and E. Tosatti, Phys. Rev. Lett. **94**, 026406 (2005).

[70] Rigorously speaking, the composite Hilbert space $\mathcal{H}_1 \otimes \mathcal{H}_2$ of fermions should be viewed as a $\mathbb{Z}_2$-graded tensor product rather than a usual tensor product. However, this distinction is unnecessary for our purpose here, as the operators under consideration are density operators involving an even number of Majorana modes.

[71] A. Hackenbroich, B. A. Bernevig, N. Schuch, and N. Regnault, Phys. Rev. B **101**, 115134 (2020).

[72] T. B. Wahl, H.-H. Tu, N. Schuch, and J. I. Cirac, Phys. Rev. Lett. **111**, 236805 (2013).

[73] G. F. Bertsch and L. M. Robledo, Phys. Rev. Lett. **108**, 042505 (2012).

[74] C. Bloch and A. Messiah, Nucl. Phys. **39**, 95 (1962).

[75] M. Wimmer, ACM Trans. Math. Softw. **38**, 1 (2012).

[76] S. Morita, R. Kaneko, and M. Imada, J. Phys. Soc. Jpn. **84**, 024720 (2015).

[77] S. R. White, Phys. Rev. Lett. **69**, 2863 (1992).